NASA Contractor Report

Helicopter Tail Rotor Blade-Vortex Interaction Noise

Albert R. George and S.-T. Chou

Sibley School of
Mechanical and Aerospace Engineering
Upson and Grumman Halls
Cornell University
Ithaca, New York

Final Technical Report
Prepared for NASA Ames Research Center
Grant NAG 2-379: Helicopter Tail Rotor Noise
Principal Investigator: A. R. George
Period: February 1, 1986 - March 31, 1987

Contents

Summary

A study is made of helicopter tail rotor noise, particularly that due to the interactions with main rotor tip vortices. This report summarizes the present analysis, the computer codes, and the results of several test cases.

Amiet's unsteady thin airfoil theory is used to calculate the acoustics of blade-vortex interaction. The noise source is modelled as a force dipole resulting from an airfoil of infinite span chopping through a skewed line vortex. To analyze the interactions between helicopter tail rotor and main rotor tip vortices, we developed a two-step approach. In the first step, the main rotor tip vortex system is obtained through a free wake geometry calculation of the main rotor using CAMRAD code developed by Johnson. This allows us to define each individual tail rotor blade-vortex interaction. In the second step, acoustic analysis takes the results from the aerodynamic interaction analysis and calculates the far-field pressure signatures for the interactions.

It is found that under a wide range of helicopter flight conditions, acoustic pressure fluctuations of significant magnitude can be generated by tail rotors due to a series of interactions with main rotor tip vortices. This noise mechanism depends strongly upon the helicopter flight conditions and the relative location and phasing of the main and tail rotors.

Introduction

During the forward flight of helicopters, tail rotors are operated in a very complicated and gusty environment containing wakes from the main rotor, fuselage, stabilizer, tail boom, etc. These wakes have significant influences on both the harmonic and the broadband noise tail rotor generates (reference 1 - 3).

Because of the size of the main rotor wakes, they are the most important sources of tail rotor noise. The main rotor wakes, which include the overall downwash flow field, the shedding vortices from blades' tips, and a number of other components have been studied in our past research (references 1 and 3). We were able to show that the overall downwash (mean and turbulent wake) of main rotor are important sources of the tail rotor harmonic and broadband noise. The main rotor tip vortex does not seem to be important to the tail rotor broadband noise. But it remains a question to be answered whether main rotor tip vortex is important to tail rotor harmonic noise and is the subject of this present study.

Because the main rotor tip vortices are strong and concentrated, they are capable of generating significant velocity perturbations to the flow field seen by the tail rotor. These strong velocity perturbations can result in large unsteady loading fluctuation on the tail rotor blades; significant noise can therefore be generated. Figure 1 shows the geometries of tail rotor blade-vortex interaction and the main rotor blade-vortex interaction. These interactions are similar in a sense since, in both cases, the blades are interacting with the vortices shed from the main rotor. However they are different because of the relative orientations. The main rotor blade-vortex interactions generally occur with vortices of near-parallel orientations (Figure 1b). They are basically transonic and have been treated by several investigators (references 4 - 8). The tail blade-vortex interactions, on the other hand, generally occur with vortices of near-normal orientations to the tail rotor plane (Figure 1c).

In the present study, the acoustics of tail rotor blade-vortex interactions is treated by the analysis of Amiet (references 9 and 10). The acoustic analysis requires input informations such as the ingested vortex properties and the vortex-blade geometric orientation. In the present study, these inputs are calculated based on a main rotor free wake geometry analysis developed by Johnson and Scully (references 11 and 12).

Acoustics of Blade-Vortex Interactions

In the present study, tail rotor blade-vortex interaction is treated as a 2-D blade vortex interaction problem (a flat plate of infinite span chopping through a moving skewed vortex). The analysis was originally developed by Amiet (references 9 and 10), who assumed that the noise source is an unsteady loading fluctuation (i.e. dipole) when a thin airfoil chops through a near normally incident vortex. The loading fluctuations can be calculated using unsteady thin-airfoil theory, and the far-field noise can then be calculated using Lowson's moving dipole theory (reference 13). Figure 2 shows the definition of the coordinates and the vortex orientation. According to Amiet, the far field pressure-time history can be calculated by

$$p(t) = \frac{i \pi \rho_0 c z U^2}{2 a_0 \sigma^2} \int_{-\infty}^{+\infty} k_x \, w(k_x,k_y) \, L(k_x,k_y,M) \, e^{i(k_x U t + \mu(Mx-\sigma)} \, dk_x$$

where ρ_0 = the density of the acoustic medium,

c = the tail rotor blade chord,

a_0 = the speed of sound,

M = U/a_0,

μ = $k_x M/(1-M^2)$,

σ^2 = $x^2+(1-M^2)(y^2+z^2)$,

L = the effective lift function, see reference 6 for details, and

w = the Fourier decomposed vortex velocity field.

In the present study, the effect of a moving vortex is included numerically, so U is the vortex normal velocity relative to the blade and can be obtained from the free wake geometry analysis (discuss later).

To be consistent with the free wake geometry analysis, a different vortex model is used compared to Amiet's original analysis. In the present study, the tangential velocity for a concentrated 2-D vortex is defined by the widely used model:

$$V_\theta = (\Gamma/2\pi r) \cdot r^2 / (r^2+r_c^2)$$

where Γ is the vortex strength, and r_c is the vortex core radius. Figure 3 shows the comparison of the vortex model used in the present study and that used by Amiet.

Since a different vortex model is used, w, the Fourier decomposed vortex velocity which is normal to the tail rotor plane, is found to be

$$w = i \tan\theta_v \Gamma r_c k_y K_1\left(r_c \sqrt{k_y^2+k_x^2/\cos^2\theta_v} \right) / \left((2\pi)^2 \sqrt{k_y^2+k_x^2/\cos^2\theta_v} \right)$$

where K_1 is the modified Bessel function of the second kind, θ_v is defined in Figure 2. It should be noted that w only accounts for the effect of the tangential velocity of the vortex; the axial flow in the main rotor tip vortices is neglected in the present analysis as discussed in the conclusion.

The acoustic pressure-time history for a given blade-vortex interaction, calculated with the present vortex model, is compared to that obtained using Amiet's original formulation. The comparison is shown in Figure 4. The results for the two different vortex models show close similarities and only minor differences. More details on the acoustics analysis can be found in references 9 and 10.

Illustrated Example and Discussion

Main Rotor Tip Vortex Free Wake Geometry

Since the main rotor tip vortex system is generally highly distorted (reference 11), classical rigid wake analysis (e.g. reference 14) can not predict the accurate locations and orientations of these vortices. The calculation of the free wake geometry of main rotor tip vortices is very important because the trajectories of vortices directly affect the characteristics of the interactions and subsequently the noise generated. In the present study, we use a comprehensive rotorcraft aerodynamics and dynamics analyses program (CAMRAD) of Johnson (reference 12) to calculate the main rotor tip vortex wake geometry. The CAMRAD code is based on a rotor-free wake geometry computation model of Scully (reference 11). Details on the CAMRAD code can be found in reference 12.

In our application, the main rotor airloads are calculated assuming non-uniform inflow at the main rotor disk, but the presence of the tail rotor is assumed to have no effect on the main rotor tip vortex system. The wakes from other part of the airframe are also neglected in the present study.

The aerodynamic analysis is aimed to provide the following information for the forthcoming acoustic analysis: the normal incident velocity of the ingested vortex relative to the tail rotor blade (U), the strength of the ingesting vortex (Γ), the skew angle between the vortex and the tail rotor axis (θ_v), and the vortex orientation with respect to the blade (ϕ_v). Refer to Figure 2 for the definitions of U, θ_v, and ϕ_v. It should be noticed that these values are generally not constant as a vortex convects through the tail rotor disk.

In this report, we will use an example to illustrate the general procedures developed in the present study. Our simulation begins with the calculation of the main rotor free wake geometry using CAMRAD. Figure 5 show the main rotor tip vortex system at four different times, this case closely represents a UH-1D helicopter in 100 knots level flight. (We use a modified version of GEOMP1 subroutine to generate the vortex location database.) From these figures, the interactions between the tail rotor and main rotor tip vortices are evident.

Trajectories of the Vortices on the Tail Rotor Plane

After the free wake geometry calculation is completed, we can find the vortex trajectory/trajectories on the tail rotor disk using program VTRAJ. VTRAJ requires the tip vortex location database and the tail rotor location to perform the interpolations. Figure 6 shows four possible patterns of the vortex trajectories on the tail rotor disk. For the 100 knots UH-1D case, only one vortex trajectory exists on the tail rotor disk and is classified to be a single vortex interaction. The vortex trajectory for this case is plotted in Figure 7,

the points shown in the figure are interpolated from the free wake geometry analysis results, and they show the locations of the vortex at different times.

Notice that the tip vortices involved in the interactions are originally shed from main rotor blades at approximately 0° azimuthal location. Figure 8 shows the definitions of azimuthal angle for both the main and the tail rotors. They are relatively "young" (less than 180° for this case), which implies that the ingested vortices are not fully rolled-up (Johnson, reference 12, had suggested that a vortex is not fully rolled-up until the vortex is older than 180° or so). Since a vortex is not fully rolled-up, the strength of the ingesting vortex should be less than the maximum bound circulation on the main rotor blade; we follow the assumption made by Scully (reference 11), and discount the strength of this partially rolled-up tip vortex by 20% from the fully grown tip vortex. For the vortex core radius, r_c, we used 0.0025 of the main rotor tip radius following the assumption of Scully (reference 11).

The results shown so far also indicate that a vortex may be chopped by more than one blade. It is quite possible that the vortex will break down immediately after the first interaction, thus subsequent interactions with the same vortex will be much weaker compared to the first one. However, the free wake geometry calculations also shows that the main rotor tip vortex is generally drifting sideways through the tail rotor disk. Therefore the next blade is likely to interact with a fresh piece of tip vortex segment, thus no effect of possible interactions with burst vortices has been included in the present study.

Detailed Definition of Tail Rotor Blade-Vortex Interactions

The informations defining a series of blade-vortex interactions can then be determine numerically by interpolating the results from main rotor free wake geometry analysis (using VINTER). Since the tail rotor RPM is generally not an integer multiplier of the main rotor RPM, the location of the blade-vortex interaction is different for each main rotor revolution. We have to locate all possible interactions until the interaction pattern repeats itself (this process usually has to go through several main rotor revolutions and is different for every helicopter configuration) to capture the general features of this phenomenon. For the first case, both #1 blades of the main and the tail rotors are set such that both blades start from $\psi = 0°$ positions initially and the computations continue through approximately four main rotor blade revolutions. Refer to Figure 8 for the definitions of main rotor and tail azimuthal angles.

Acoustic Signature Calculation

For the 100 knot UH-1D case, the data defining a series of blade-vortex interactions (which we had obtained in the previous section) are now used as the inputs for the noise

calculation (program VNOISE). The results are plotted in Figure 9. The results are given in term of the pressure-time history, the pressure is in Pascal (N/m2), and the horizontal axis is the time axis (tick marks are 0.1 seconds apart).

It should be notice that the pressure peaks are not separated by equal time intervals; therefore if one Fourier analyzed the pressure-time history, the resulting acoustic spectrum will behave more like broadband noise with widened spectrum peaks rather than pure harmonics. Also an interaction with higher normal velocity (advancing blades or near the blade tip) will result in a stronger but relatively short perturbation pressure peak; while an interaction characterized by smaller normal velocity (retreating blades or near the blade hub) will result in a weaker but more lasting pressure perturbation.

In references 2 and 3, we have shown that these types of tail rotor blade-vortex interactions exist even at lower helicopter speeds. Although the overall vortex convection speed decreases with the lower helicopter airspeed, the interactions are more frequent. Also because the strength of the vortex has to increase at lower airspeed to generate the required lift, the magnitude of the acoustic pressure fluctuation does not seem to change much compared to the high speed case. Details of this study can be found in references 2 and 3.

Additonal Examples

Effect of Tail Rotor Location

As discussed previously, the vortex trajectory on the tail rotor disk is very important to the blade-vortex interaction noise. The tail rotor location relative to the main rotor, and the helicopter operating conditions are two primary variables that change the vortex trajectories on the tail rotor disk. To illustrate the effect of tail rotor location on the blade-vortex interaction noise, we will artificially lower the UH-1D tail rotor by 0.5 m.

For the same 100 knots level flight case, the main rotor tip vortex trajectory on the tail rotor disk is now shown in Figure 10. Notice that the vortex path is higher than that shown in Figure 7 due to a lowered tail rotor and hence causing the blade-vortex interactions to occur with advancing tail rotor blades. Following the procedures described earlier, the interaction locations and vortex properties can again be determined using VINTER. The acoustic pressure signatures of the tail rotor blade-vortex interactions can also be calculated, the results are shown in Figure 11.

There are considerable differences between the results shown in Figures 9 and 11. Since the vortex is passing through the advancing side of the tail rotor, this results a higher relative velocity between the tail rotor blade and the ingesting vortex element, so in general the pressure perturbation has higher peaks. Also the interactions are more frequent than in the previous cases. Unquestionably, with this configuration (lowered tail rotor), the overall tail rotor noise will be more significant than that from a standard tail rotor.

Comparison with Experiments

The most important helicopter tail rotor noise experiments we have examined are those of Balcerak (reference 15). In a parametric study, he found that the noise increased as the main rotor wake passed the tail rotor. His tests employed a model-scale (1/16th) UH-1 helicopter and input parameters are well-defined. Here, we will compare the present analysis to his experimental data.

The case we chose to simulate corresponds to an advance ratio of 0.2. First, the main rotor free wake geometry was calculated using CAMRAD. The results are presented in Figure 12. Unlike from the full-scale UH-1D case, the model-scale calculations show multiple vortex trajectories on the tail rotor disk (Figure 13). The two vortex trajectories present on the tail rotor disk look similar but are quite different. The first trajectory (the upper one) was shed originally from approximately 0° main rotor blade location, the vortex segments on this path are relatively young, just like that in the full-scale UH-1D case. The second (the lower) trajectory, on the other hand, was shed from the 180° main rotor azimuthal position. The vortices on this path are much older than those on the upper

passage (their ages are approximately 540° or older), and will be fully grown vortices (compared to those partially rolled-up vortices as on the upper passage).

In most of Balcerak's tests, the model scale UH-1 tail rotor is rotating at an integer multiple of main rotor speed (main rotor 2120 RPM, tail rotor 10600 RPM for our case). The phasing of the tail rotor may have some impact on the overall noise generation; this will be discussed later. In the first example, we will assume zero phasing difference between the two rotors (both #1 blades start from 0° azimuthal locations). With this phasing, a set of blade-vortex interactions can be defined and the acoustic signatures calculated. Figure 14 shows the acoustic results for this zero phasing case.

Figure 15 shows the pressure signature and the corresponding noise spectrum for another zero phase difference case with a slightly lower tail rotor location, along with the experimental results of Balcerak (reference 15). The results compare fairly well with the experiment, considering that the experiment's tail rotor phasing was not known.

Effect of Tail Rotor Phasing

In this section we will examine the effect of different main/tail rotor phasings on the tail rotor blade-vortex interaction noise. Four more different tail rotor/main rotor phasings are examined for the case of Figure 14. In all cases, the #1 blade of the main rotor starts from the same azimuthal position (0°), but the tail rotor #1 blade starts from 30°, 60°, 90°, and 135° respectively. Since the main rotor free wake geometry stays the same as the zero phasing case, the first step (CAMRAD) and the second step (VTRAJ, locating the vortex trajectories) will be skipped. Only VINTER (to define blade-vortex interactions sequence) and VNOISE (to calculate the acoustic pressure signatures) are to be rerun. The acoustic results are presented in Figures 16 - 19. It is obvious that tail rotor/main rotor phasing can be very important; in the test cases presented, it not only affects the frequency of the interactions, it also affects the signal strengths of each interactions.

Conclusions

Tail rotor blade-main rotor tip vortex interaction is a very important tail rotor noise mechanism. The noise generated depends strongly on the main rotor operating conditions and on the tail rotor location and its phasing. Major parameters governing this blade-vortex noise generation are the ingested vortex strength, the ingested vortex skew angle relative to the blade, and the relative velocity of the ingested vortex to the tail rotor blade. More detailed study should be devoted to the problem considering a vortex chopped by an airfoil of finite span.

It is clear that the main and tail rotor relative phasing and location have a strong influence on the noise tail rotor generates. They offer opportunities to reduce tail rotor blade-vortex interaction noise by controlling the phasing and the relative location of the main and tail rotors. However, more work is needed to demonstrate the full potential of these techniques.

The present study does not include the possibly major effect of the axial flow in the main rotor tip vortex. This can be another strong contributor to the unsteady loading fluctuation on a tail rotor blade. The result of free wake geometry analysis does indicate some evidence of the main rotor tip vortex drifting normal to the tail rotor disk. Also the strength of main rotor tip vortex is not constant, this will result in an axial pressure gradient inside the vortex, thus inducing some axial flow. These important problems should be addressed in future studies.

References

1. George, A. R., Chou, S.-T.: A Comparative Study of Tail Rotor Noise Mechanisms. Journal of the American Helicopter Society, Vol. 31, No. 4, 1986, pp. 36-42.

2. Chou, S.-T., George A. R.: Progress in Helicopter Tail Rotor Noise Analysis. Proceedings of the 42nd Annual Forum of the American Helicopter Society, Washington, D.C., June 1986; also AIAA-86-1900, AIAA 10th Aeroacoustics Conference, Seattle, Washington, July 1986.

3. Chou, S.-T.: A Study of Rotor Broadband Noise Mechanisms and Helicopter Tail Rotor Noise. Ph.D. thesis, Cornell University, Ithaca, New York, May 1987.

4. George, A. R. and Chang, S. B.: Noise Due to Transonic Blade-Vortex Interactions. 39th Annual National Forum of the American Helicopter Society, St. Louis, Missouri, May 1983.

5. George, A. R. and Chang, S. B.: Flow Field and Acoustics of Two-Dimensional Transonic Blade-Vortex Interactions. AIAA-84-2309, AIAA/NASA 9th Aeroacoustics Conference, Williamsburg, Virginia, October 1984.

6. George, A. R. and Lyrintzis, A. S.: Mid- and Far-Field Calculations of Blade-Vortex Interactions. AIAA-86-1954, AIAA 10th Aeroacoustics Conference, Seattle, Washington, July 1986.

7. Srinivasan, G. R., McCroskey, W. J., and Kutler, P.: Numerical Simulation of the Interaction of a Vortex with a Stationary Airfoil in Transonic Flow. AIAA-84-0254, AIAA 22nd Aerospace Sciences Meeting, Reno, Nevada, January 1984.

8. McCroskey, W. J., Yu, Y. H., and Smetana, F. O.: Workshop on Blade-Vortex Interactions. NASA Ames Research Center, October 1984.

9. Schlinker, R. H., Amiet, R. K.: Rotor-Vortex Interaction Noise. NASA CR-3744, October 1983.

10. Amiet, R. K.: Airfoil Gust Response and the Sound Produced by Airfoil-Vortex Interaction. Journal of Sound and Vibration, Vol. 107, No. 3, June 1986.

11. Scully, M. P.: Computation of Helicopter Rotor Wake Geometry and its Influence on Rotor Harmonic Airloads. M.I.T. ASRL Report TR-178-1, Cambridge, Massachusetts, March 1975.

12. Johnson, W.: A Comprehensive Analytical Model of Rotorcraft Aerodynamics and Dynamics, Part I, II, and III. NASA TM's 81182, 81183, and 81184, 1980.

13. Lowson, M. V.: The Sound Field for Singularities in Motion. Proceedings of the Royal Society of London, Series A, Vol. 286, 1965.

14. Heyson, H. H.: Nomographic Solution of the Momentum Equation for VTOL-STOL Aircraft. NASA TN-D-814, 1961.

15. Balcerak, J. C.: Parametric Study of the Noise Produced by the Interaction of the Main Rotor Wake and Tail Rotor. NASA CR-145001, 1976.

Publications Issued During the Research

1. George, A. R., Chou, S.-T.: A Comparative Study of Tail Rotor Noise Mechanisms. Journal of the American Helicopter Society, Vol. 31, No. 4, 1986, pp. 36-42.

2. Chou, S.-T., George A. R.: Progress in Helicopter Tail Rotor Noise Analysis. Proceedings of the 42nd Annual Forum of the American Helicopter Society, Washington, D.C., June 1986.

3. Chou, S.-T., George A. R.: Helicopter Tail Rotor Noise. AIAA-86-1900, AIAA 10th Aeroacoustics Conference, Seattle, Washington, July 1986.

4. Chou, S.-T.: A Study of Rotor Broadband Noise Mechanisms and Helicopter Tail Rotor Noise. Ph.D. thesis, Cornell University, Ithaca, New York, May 1987.

5. Chou, S.-T., George A. R.:Helicopter Tail Rotor Blade-Vortex Interaction Noise. Proceedings, NOISE-CON 1987, Penn State University, June, 1988.

6. George, A. R., Chou, S.-T.: Helicopter Tail Rotor Blade-Vortex Interaction Noise. Final Technical Report, NASA Grant NAG 2-379, Period: February 1, 1986 - March 31, 1987.

List of Figures

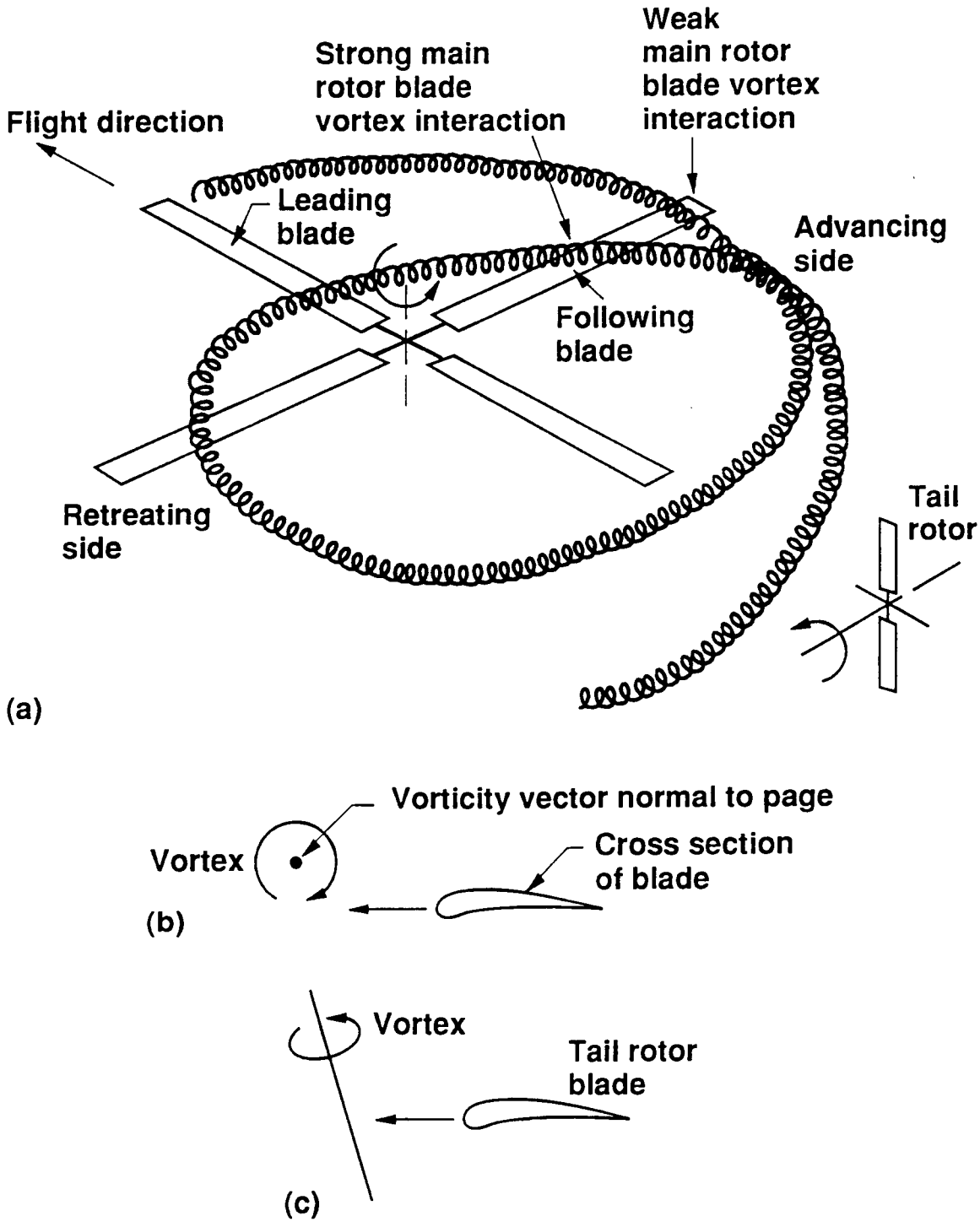

Figure 1. Geometry of Helicopter Blade-Vortex Interactions (from reference 9).
(a) Illustration of the Relative Location of the Helicopter Main Rotor Tip Vortex System and the Tail Rotor.
(b) Illustration of the Parallel Main Rotor Blade-Vortex Interaction.
(c) Illustration of the Skewed Tail Tail Rotor Blade-Vortex Interaction.

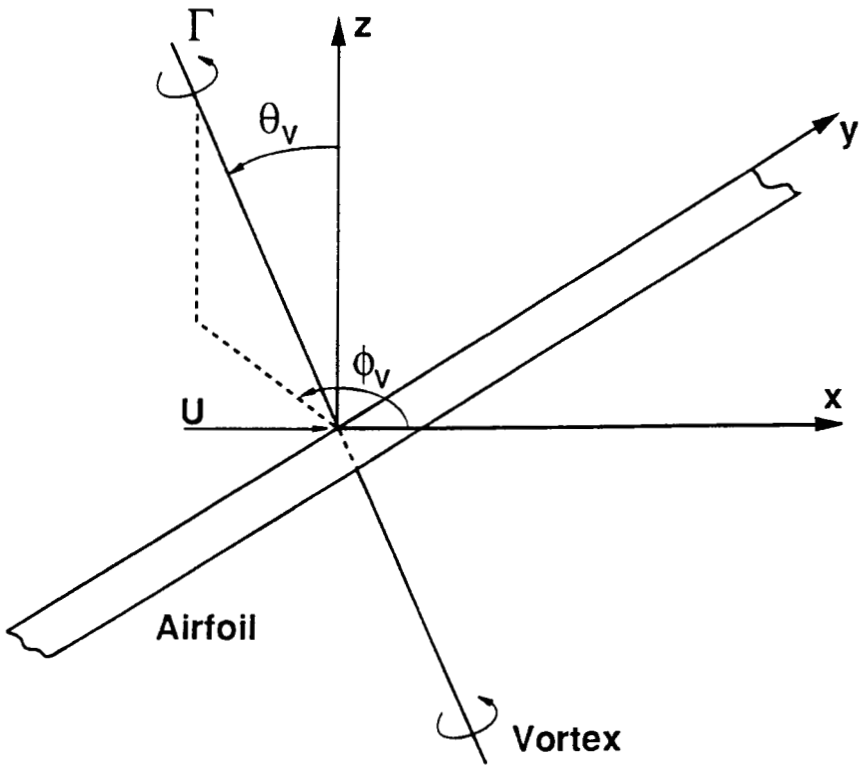

Figure 2. Sketch of the 2-Dimensional Near-Normal Blade-Vortex Interaction.

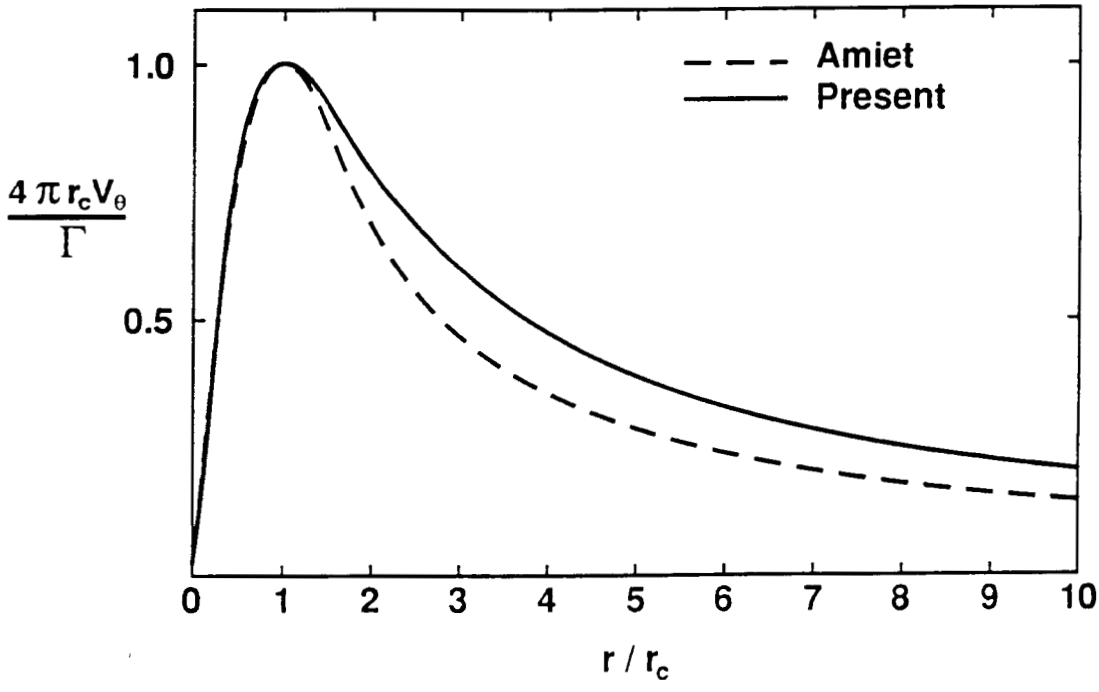

Figure 3. Comparison of the Tangential Velocity Distribution for Different Vortex Models.

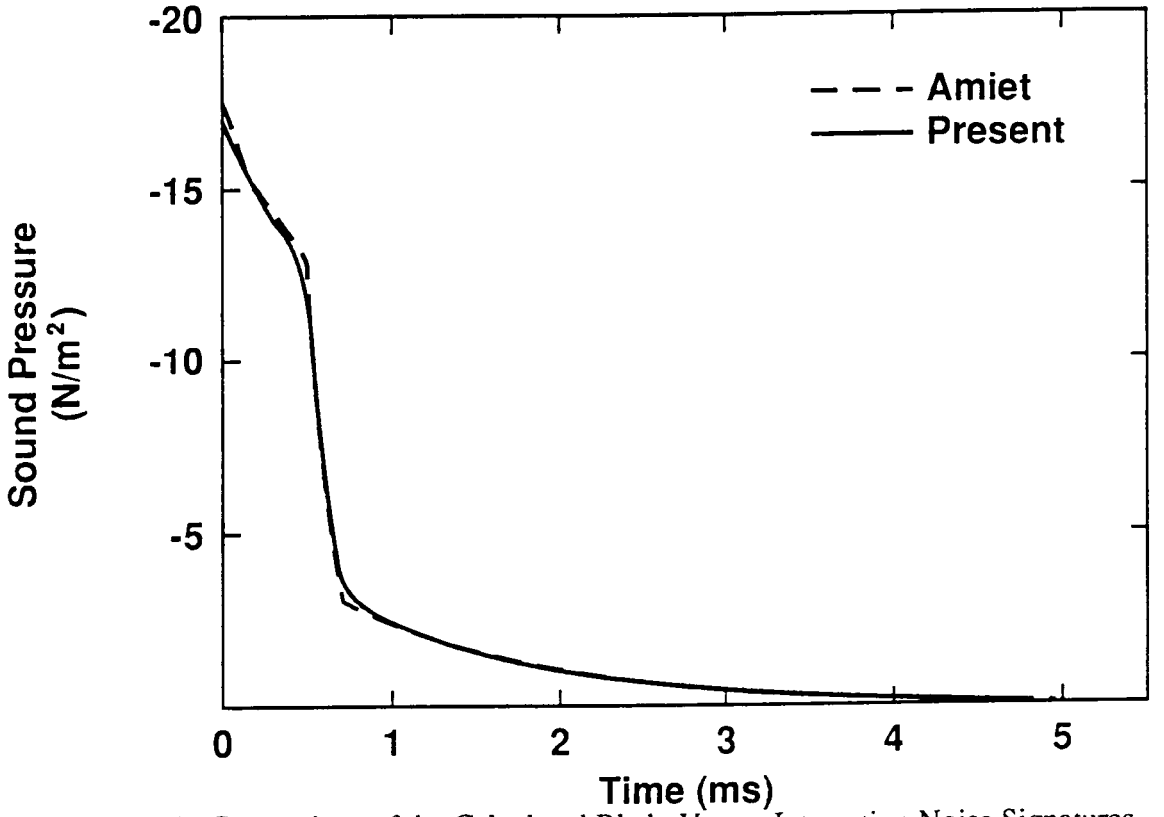

Figure 4. Comparison of the Calculated Blade-Vortex Interaction Noise Signatures Using Different Vortex Models.

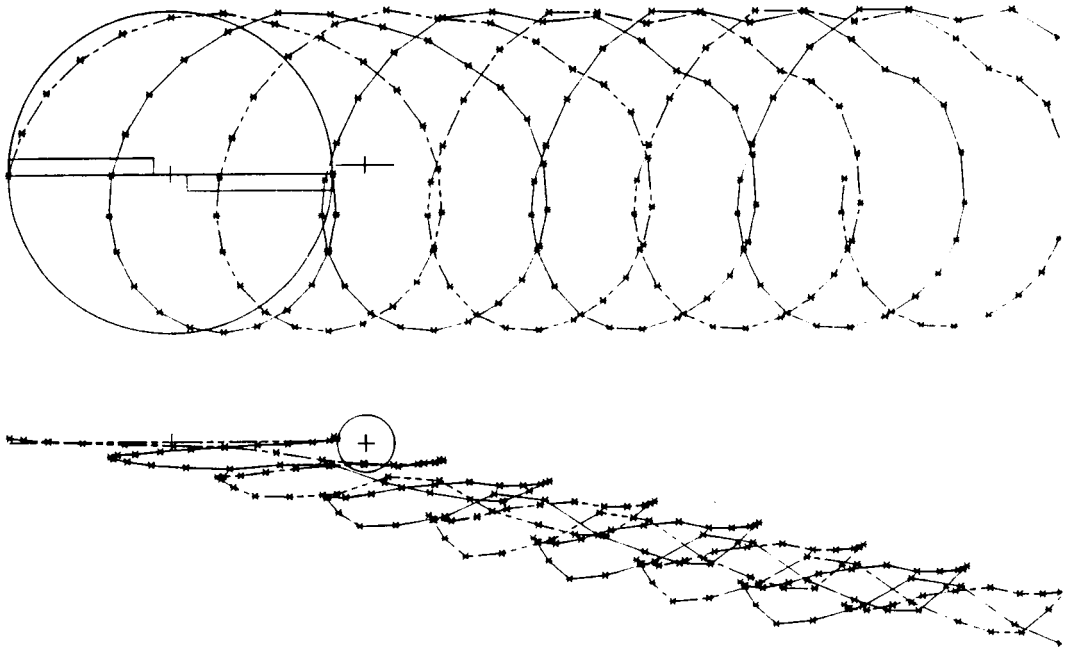

Figure 5. Calculated UH-1D Free Wake Geometry Results, 100 Knot Level Flight.
(a) Main Rotor $\psi = 0°$.

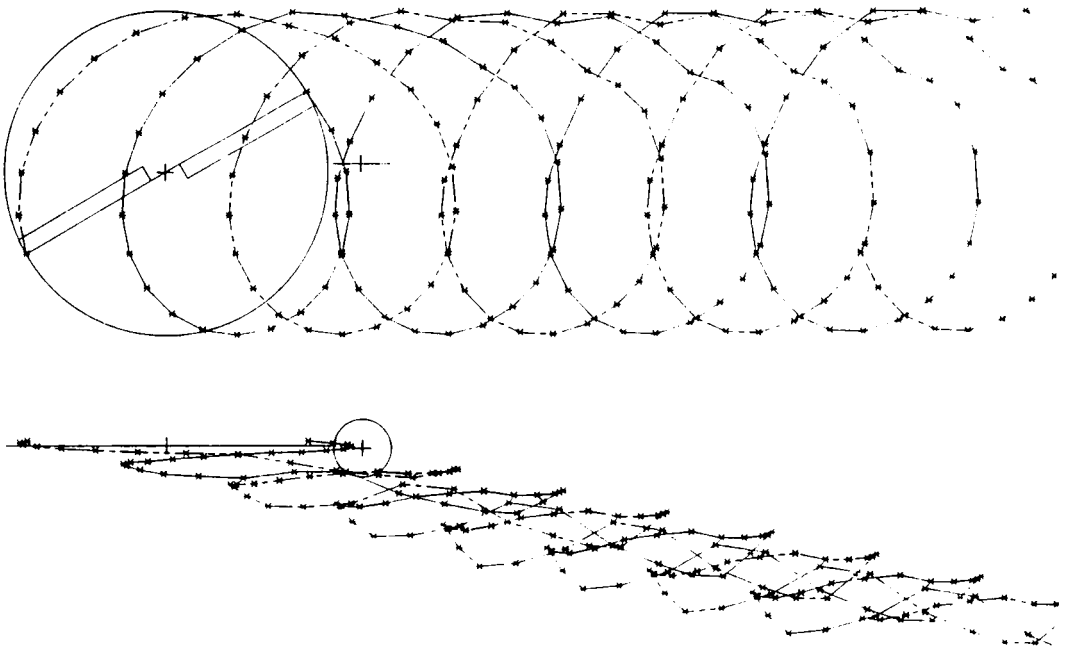

Figure 5. Calculated UH-1D Free Wake Geometry Results, 100 Knot Level Flight.
(b) Main Rotor $\psi = 30°$.

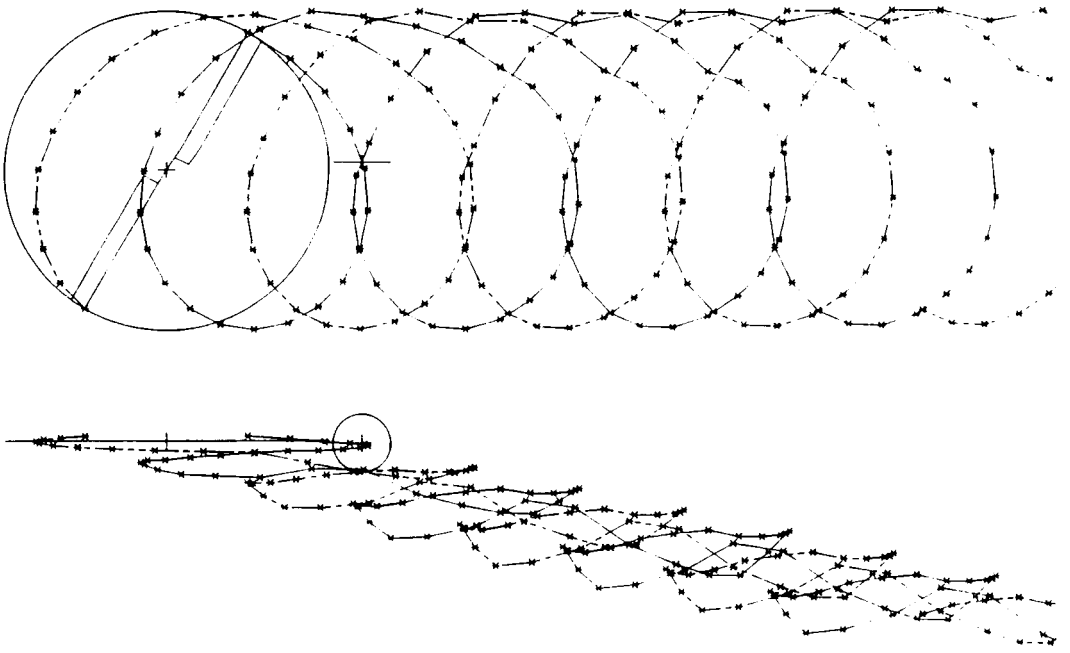

(c) Main Rotor $\psi = 60°$.

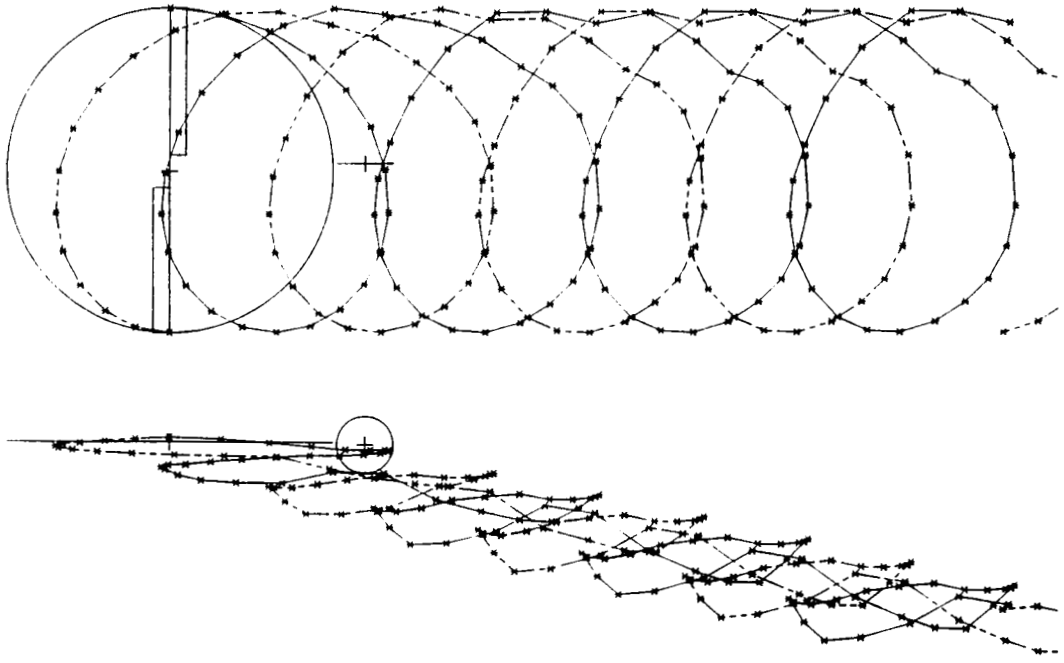

Figure 5. Calculated UH-1D Free Wake Geometry Results, 100 Knot Level Flight.
(d) Main Rotor $\psi = 90°$.

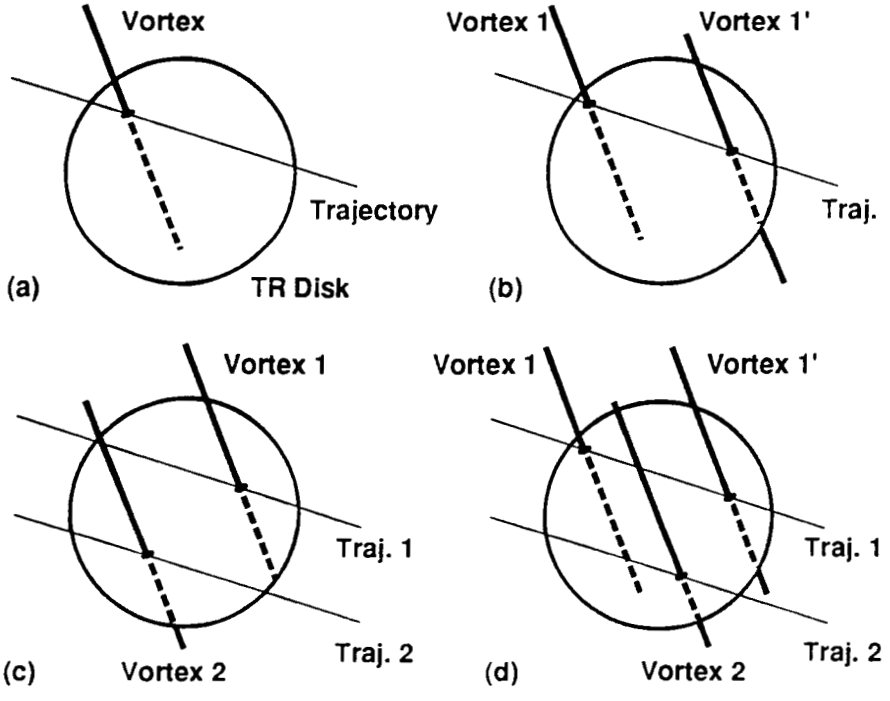

Figure 6. Possible Main Rotor Tip Vortex Trajectory Patterns on the Tail Rotor Disk.

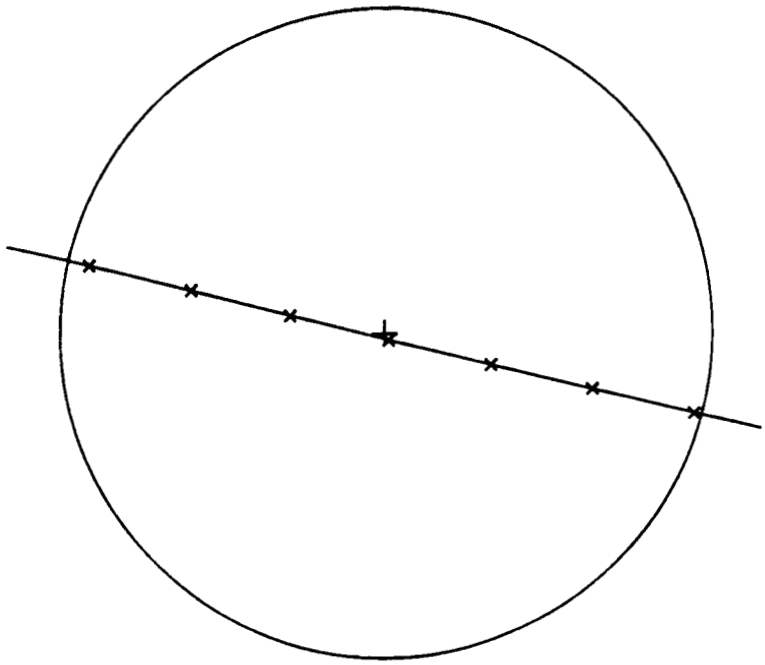

Figure 7. Calculated Main Rotor Tip Vortex Trajectory on the Tail Rotor Disk, UH-1D 100 Knot Level Flight.

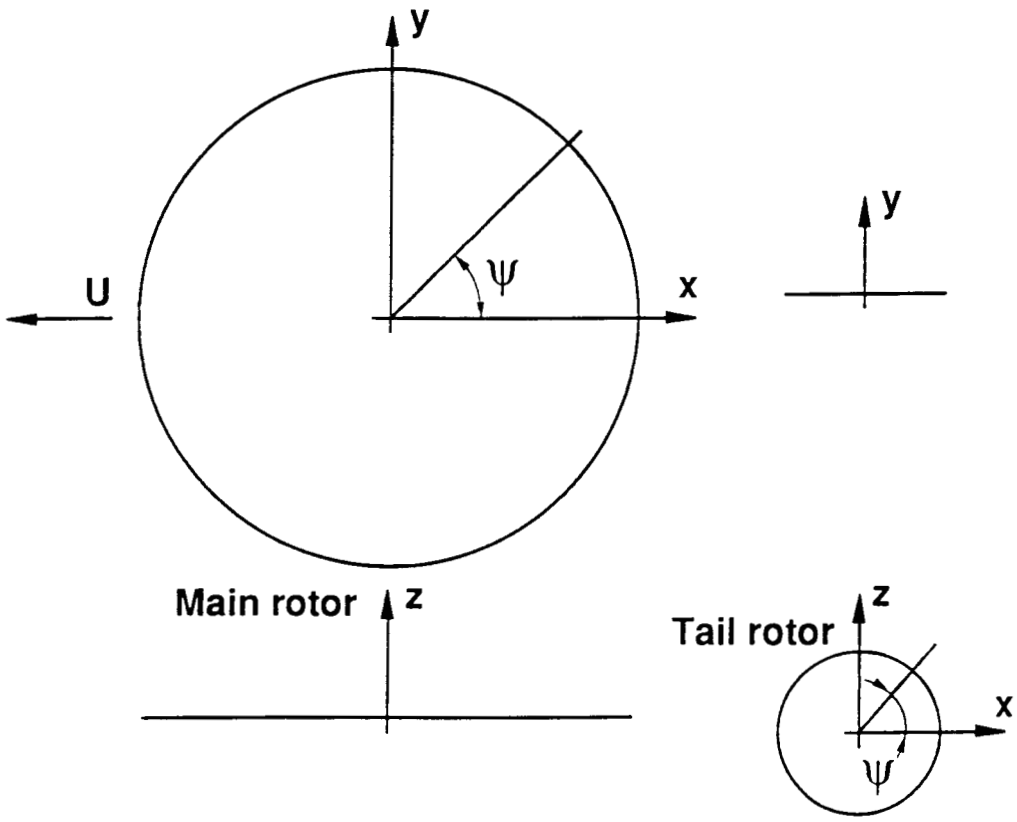

Figure 8. Definitions of the Main Rotor and Tail Rotor Coordinates.

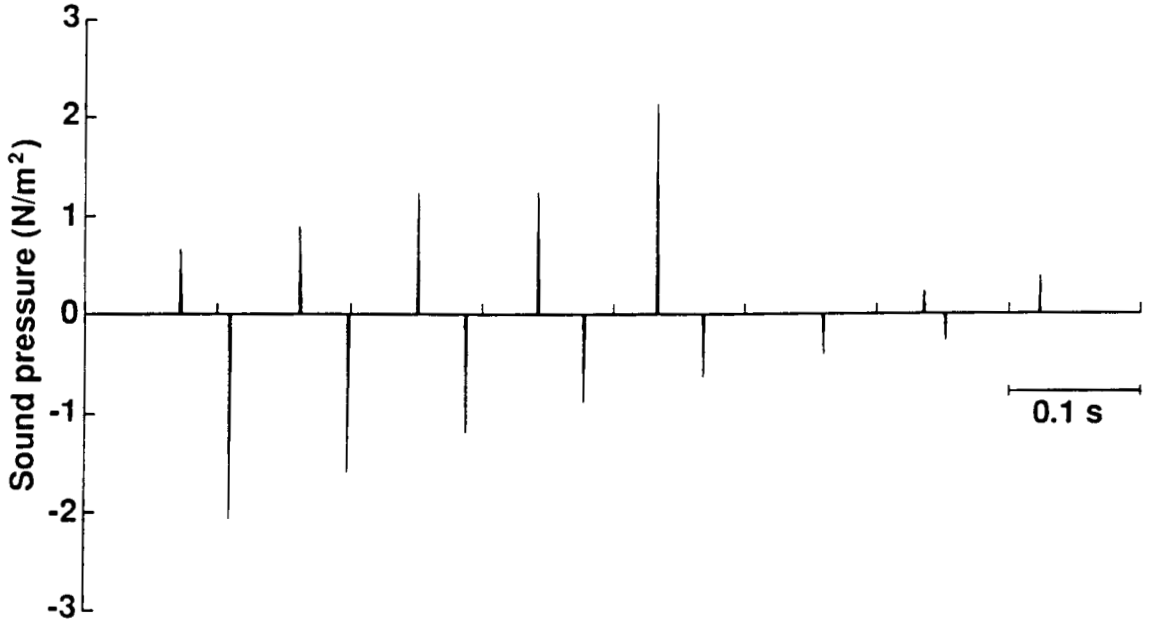

Figure 9. Calculated Noise Signature for the Tail Rotor Blade-Vortex Interactions, UH-1D 100 Knot Level Flight.

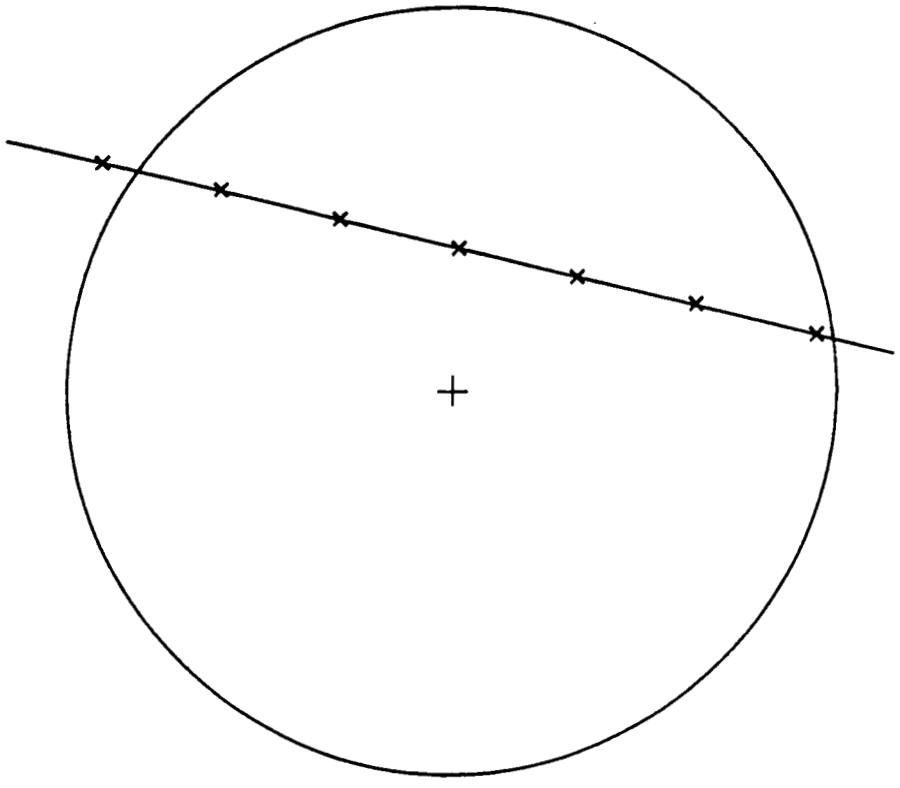

Figure 10. Main Rotor Tip Vortex Trajectory on the Tail Rotor Disk, UH-1D 100 Knot Level Flight, Tail Rotor is Lowered by 0.5 Meters.

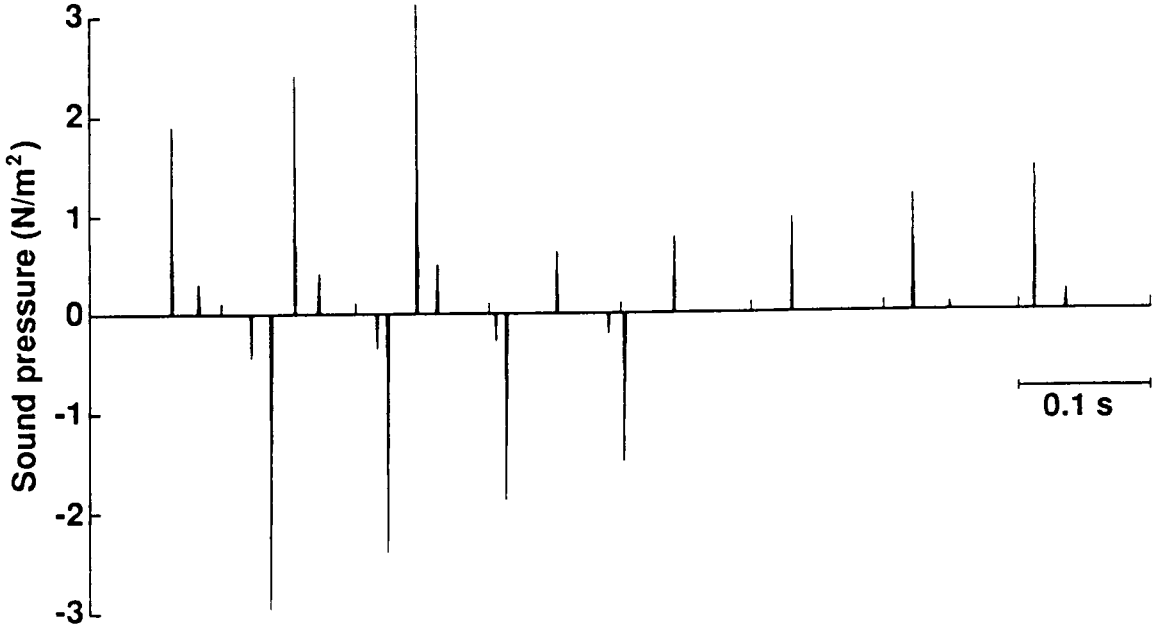

Figure 11. Calculated Noise Signature for the Tail Rotor Blade-Vortex Interactions, UH-1D 100 Knot Level Flight, Tail Rotor is Lowered by 0.5 Meters.

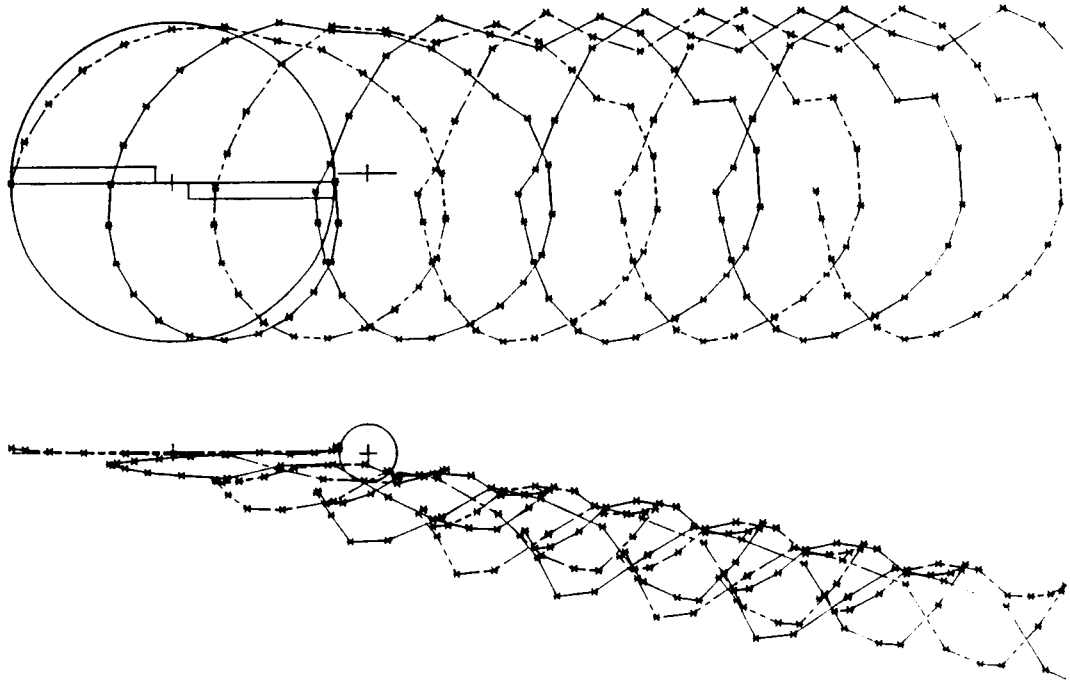

Figure 12. Calculated Model Scale UH-1 Free Wake Geometry Results, $\mu = 0.2$ Level Flight.

(a) Main Rotor $\psi = 0°$.

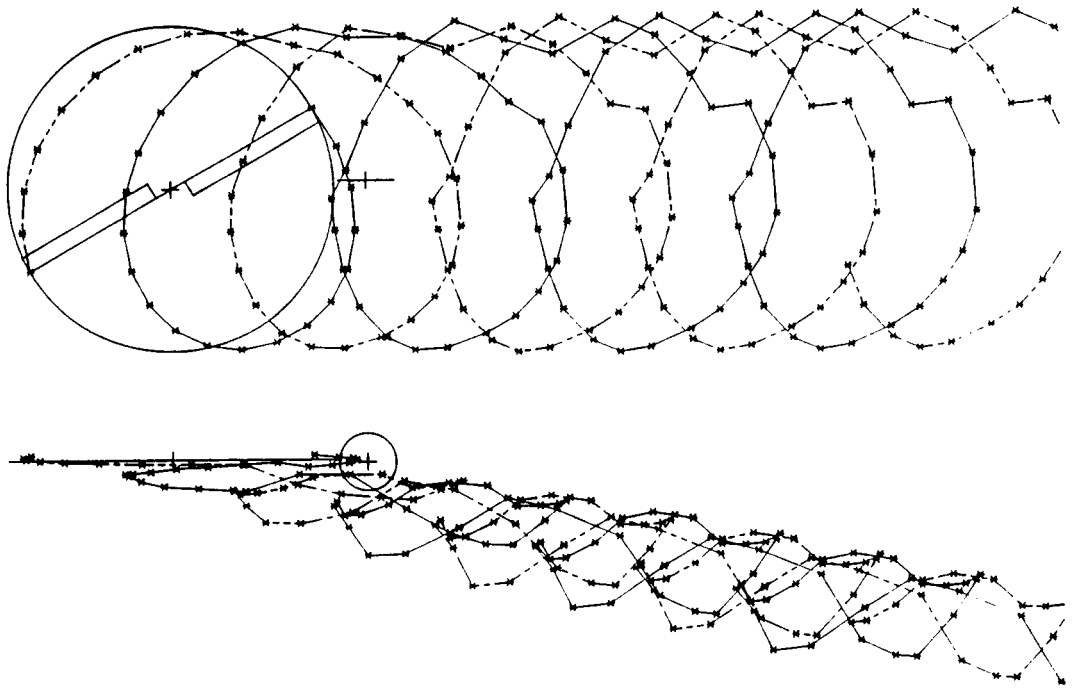

Figure 12. Calculated Model Scale UH-1 Free Wake Geometry Results, $\mu = 0.2$ Level
(b) Main Rotor $\psi = 30°$.

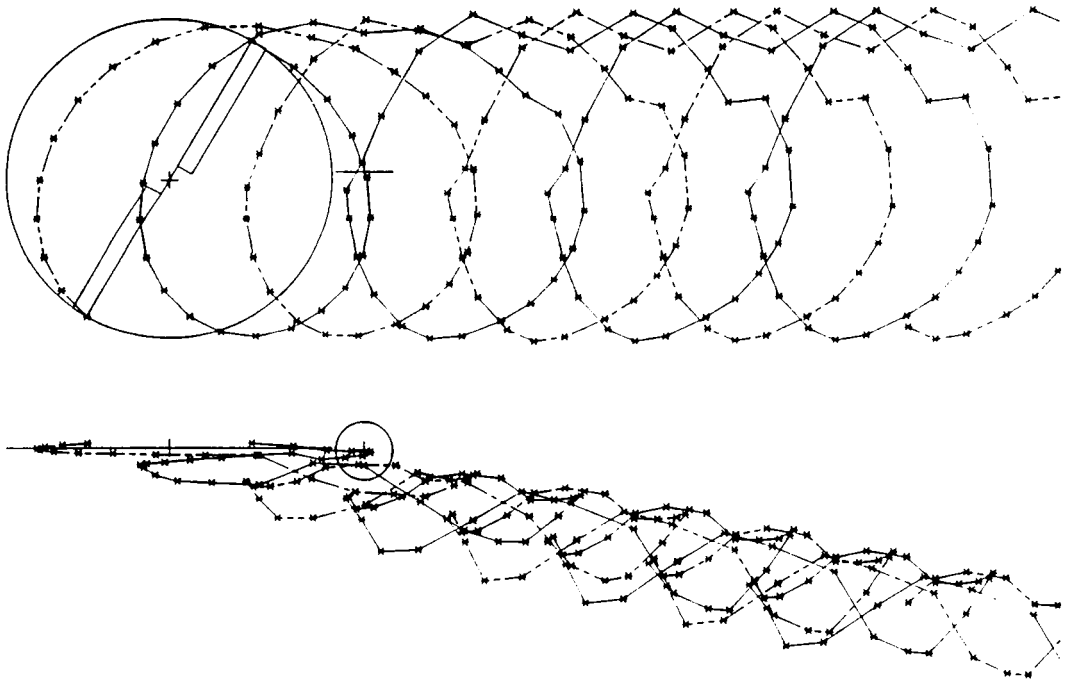

(c) Main Rotor $\psi = 60°$.

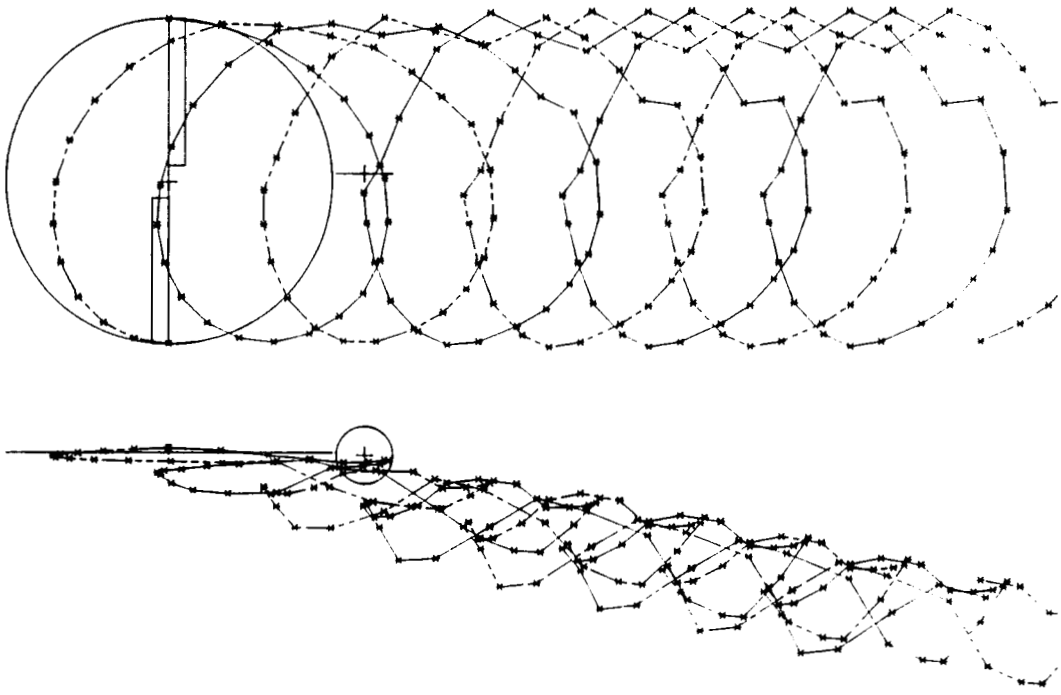

Figure 12. Calculated Model Scale UH-1 Free Wake Geometry Results, $\mu = 0.2$ Level
(d) Main Rotor $\psi = 90°$

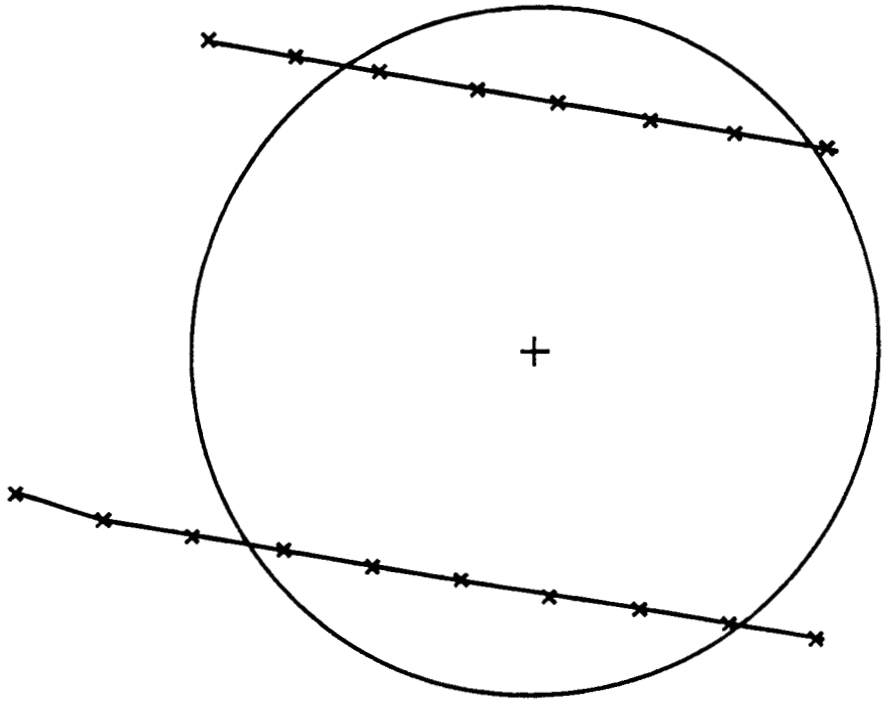

Figure 13. Main Rotor Tip Vortex Trajectories on the Tail Rotor Disk, Model Scale UH-1, $\mu = 0.2$ Level Flight.

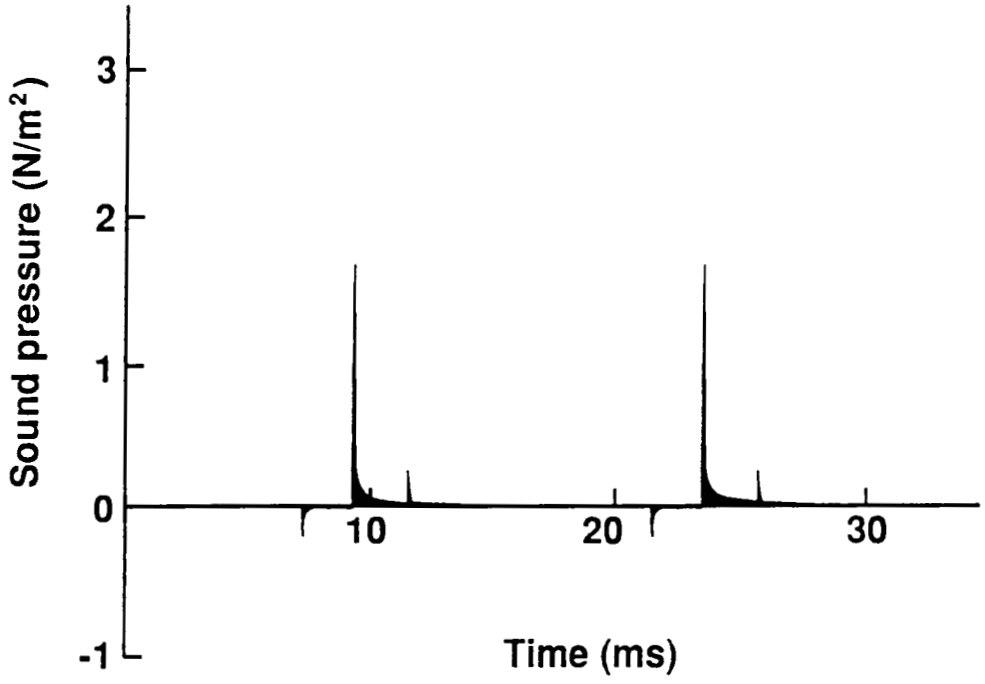

Figure 14. Calculated Noise Signature for the Tail Rotor Blade-Vortex Interactions, Model Scale UH-1, $\mu = 0.2$ Level Flight, Synchronized Main and Tail Rotors (Zero Phase Shift).

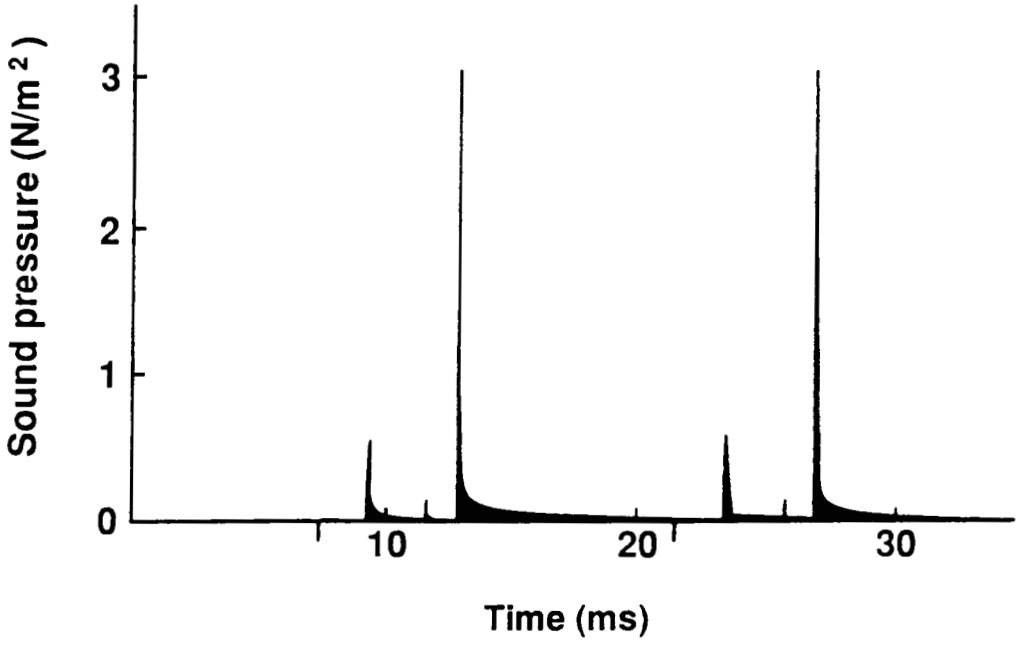

Figure 15. Comparison of Calculated Tail Rotor Blade-Vortex Interaction Spectrum and the Experiment Results of Balcerak (reference 15), Model Scale UH-1, $\mu = 0.2$ Level Flight. Slightly Lowered Tail Rotor Position.

(a) Calculated Signature.

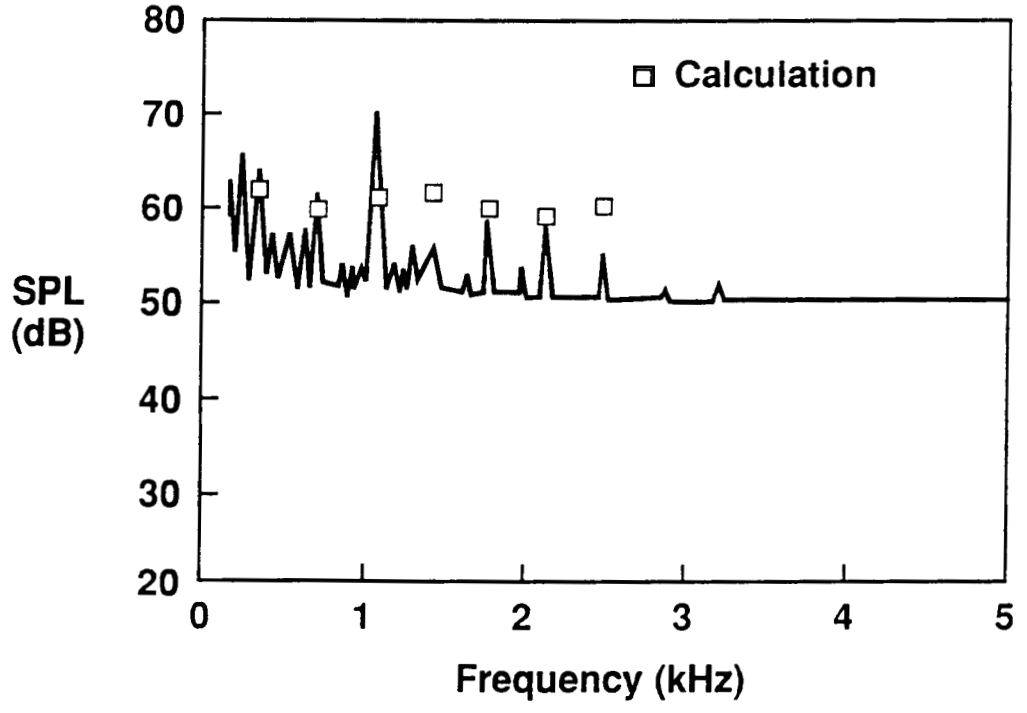

Figure 15. Comparison of Calculated Tail Rotor Blade-Vortex Interaction Spectrum and the Experiment Results of Balcerak (reference 15), Model Scale UH-1, $\mu = 0.2$ Level Flight. Slightly Lowered Tail Rotor Position.

(b) Calculated Spectrum and Experimental Results.

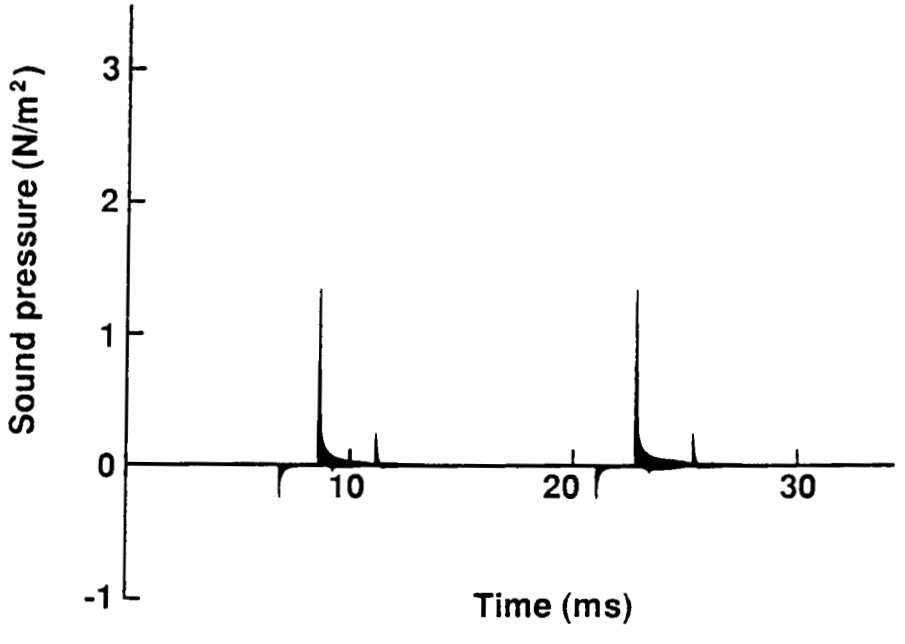

Figure 16. Calculated Noise Signature for the Tail Rotor Blade-Vortex Interactions, Model Scale UH-1, $\mu = 0.2$ Level Flight, Synchronized Main and Tail Rotors (30° Phase Shift).

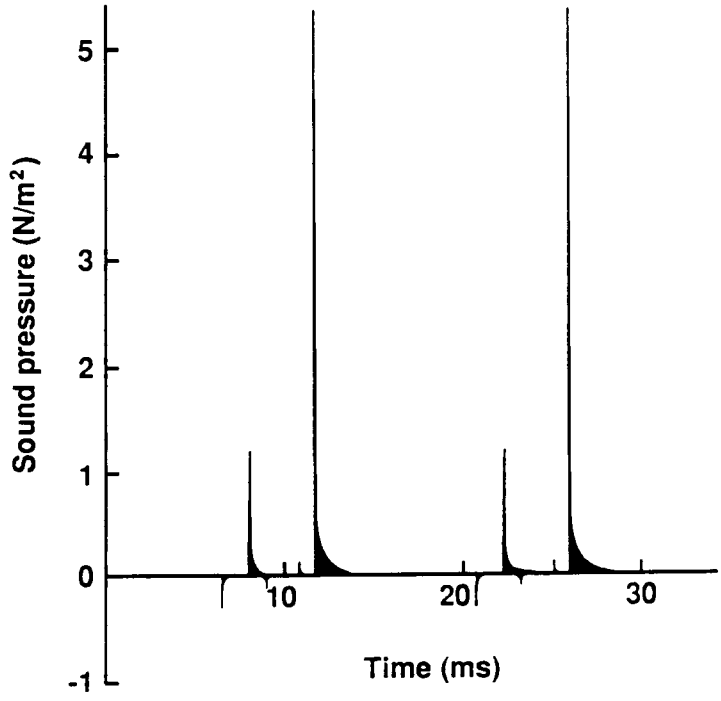

Figure 17. Calculated Noise Signature for the Tail Rotor Blade-Vortex Interactions, Model Scale UH-1, $\mu = 0.2$ Level Flight, Synchronized Main and Tail Rotors (60° Phase Shift).

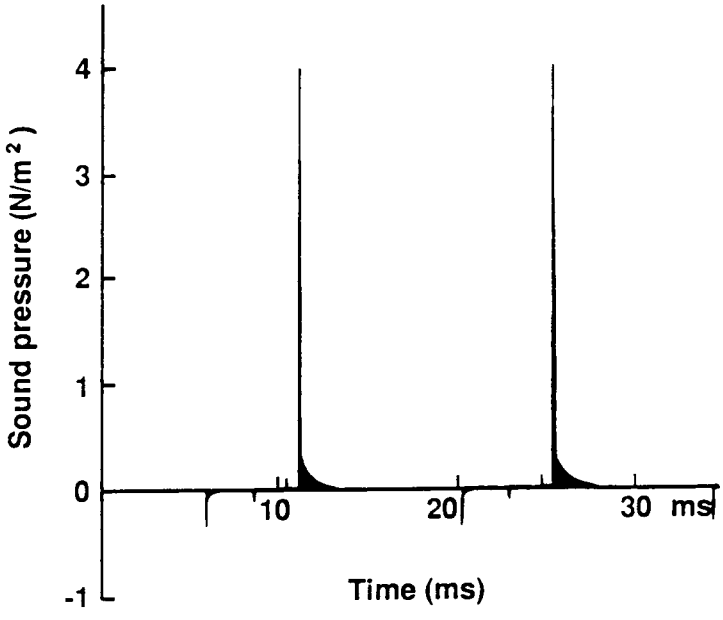

Figure 18. Calculated Noise Signature for the Tail Rotor Blade-Vortex Interactions, Model Scale UH-1, $\mu = 0.2$ Level Flight, Synchronized Main and Tail Rotors (90° Phase Shift).

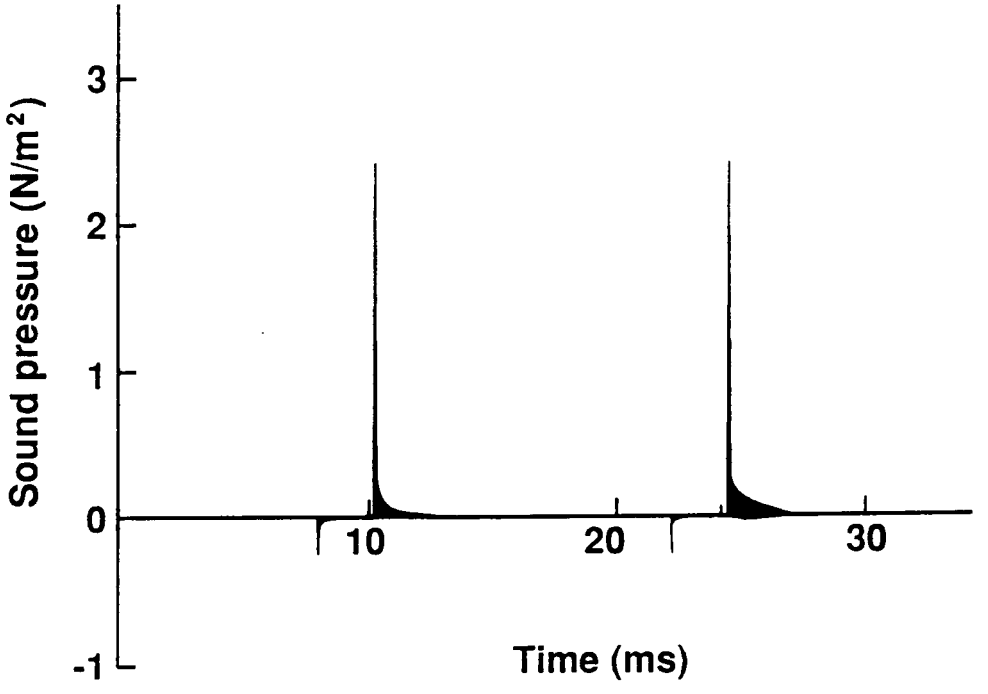

Figure 19. Calculated Noise Signature for the Tail Rotor Blade-Vortex Interactions, Model Scale UH-1, $\mu = 0.2$ Level Flight, Synchronized Main and Tail Rotors (135° Phase Shift).